The Preparation, Structures, and Properties of Poly(vinylidene fluoride)/Multiwall Carbon Nanotubes Nanocomposites

Xue-Gang Tang,[1] Meng Hou,[1] Lei Ge,[2] Jin Zou,[1,3] Rowan Truss,[1,2] Wei Yang,[4] Ming-Bo Yang,[4] Zhong-Hua Zhu,[2] Rui-Ying Bao[4]

[1]*School of Mechanical and Mining Engineering, The University of Queensland, Brisbane, QLD 4072, Australia*
[2]*School of Chemical Engineering, The University of Queensland, Brisbane, QLD 4072, Australia*
[3]*Centre for Microscopy and Microanalysis, The University of Queensland, Brisbane, QLD 4072, Australia*
[4]*College of Polymer Science and Engineering, State Key Laboratory of Polymer Materials Engineering, Sichuan University, Chengdu, Sichuan 610065, China*

Received 13 August 2010; accepted 16 December 2011
DOI 10.1002/app.36671
Published online 2 February 2012 in Wiley Online Library (wileyonlinelibrary.com).

ABSTRACT: Poly(vinylidene fluoride) (PVDF)/multiwall carbon nanotubes (MWCNTs) were prepared by a phase inversion technique. Long chain macromolecules, maleic anhydride grafted PVDF (PVDF-MAH) were used to fine tune the interface. Transmission electron microscopy (TEM) images revealed that the MWCNTs are quasi-homogeneously dispersed in the PVDF matrix. The results of differential scanning calorimetry (DSC) and attenuated total reflectance Fourier transform infrared spectroscopy (ATR-FTIR) showed that the addition of MWCNTs induced β-phase PVDF, and both the melting behavior and crystal structures of PVDF did not change obviously by the addition of MWCNTs. However, the addition of long chain macromolecules PVDF-MAH did not alter the crystal structure according to the ATR-FTIR test, but significantly changed the melting behavior as evidenced by a multiple melting behavior detected by DSC. Dynamic mechanical analysis (DMA) tests showed that both the addition of MWCNTs and PVDF-MAH increased the storage modulus and the improvement of nanocomposites was better at low temperature regions than high temperature regions. In addition, no significant change of the T_g was observed with the addition of MWCNTs and PVDF-MAH. Tensile tests showed that the addition of MWCNTs and PVDF-MAH increased the modulus and tensile strength. Creep test showed that the addition of MWCNTs can increase the creep stability. However, the interfacial modification here was not enough to change the creep behavior significantly. J Appl Polym Sci 125: E592–E600, 2012

Key words: multiwall carbon nanotubes; poly(vinylidene fluoride); creep behavior; phase inversion technique

INTRODUCTION

Since their discovery by Iijima,[1] a number of exotic physical properties of carbon nanotubes (CNTs) have been observed. Research has shown that the Young's modulus for CNTs is superior to all carbon fibers with a value greater than 1 TPa,[2] while the highest strength measured is 63 GPa.[3] Even the weakest type of CNTs have strengths of several GPa.[4] Another advantage for CNTs is the high aspect ratio, which have diameters ranging from 1 to 100 nm and lengths of up to several millimetres.[5] This combined with the properties makes CNTs ideal candidates as advanced filler materials in composites.[6–11]

There are four main requirements for effective reinforcement. These are a large aspect ratio, good dispersion, alignment, and interfacial stress transfer.[9,12,13] Dispersion is a fundamental issue. Uniformly dispersed CNTs coated with polymer is imperative to achieve efficient load transfer to the nanotube network, which results in a more uniform stress distribution and minimizes the presence of stress-concentration centres. The dispersion of CNTs can be achieved by controlling the processing using solution method with functionalized CNTs or an ultrasonic treatment.[14] Normally there are several ways to fabricate polymer CNTs nanocomposites: (1) solution mixing, (2) *In situ* polymerization,[15] or (3) melt processing.[16] The solution method is the most common method for fabricating polymer nanocomposites because good dispersion can be obtained by the selection of solvent and treatment of the carbon nanotubes. At the same time, further interfacial modification can be achieved easily in solution. However, large amounts of solvent are used in this method, most of which is not friendly with the

Correspondence to: M. Hou (m.hou@uq.edu.au).
Contract grant sponsors: IPRS (Endeavour International Postgraduate Research Scholarship, Australia), UQRS (University of Queensland Research Scholarship), UQ New Staff Research Start-up Found.

environment. In addition, traditional solution methods need a long time to evaporate the solvent, which may result in the CNTs reagglomerate during slow solvent evaporation, leading to inhomogeneous distribution of the CNTs in the polymer matrix. *In situ* polymerization is ideal for the creation of polymer/CNTs nanocomposites because of the free radical initiated, addition chain reaction of vinyl monomers at a molecular level.[14] However, as polymerization progressing, the viscosity of the reaction medium increases, and the extent of *in situ* polymerization reactions might be limited.[17] Melt blending uses high temperature and high shear forces to disperse nanotubes in a polymer matrix and is most compatible with current industrial practices. However, relative to solution blending methods, melt blending is generally less effective in dispersing nanotubes in polymers and is limited to lower concentrations due to the high viscosities of the composites at higher nanotube loadings.[17] Consequently, it remains a challenge to develop methods to fabricate polymer carbon nanotube nanocomposites, which are friendly to the environment, with good dispersion, high material outputs.

Poly(vinylidene fluoride) (PVDF) is a semicrystalline polymer with a variety of interesting properties. PVDF has been a widely studied polymer because of its potential as piezoelectric and pyroelectric materials. These properties, combined with high elasticity and processing ability, provide a variety of technological applications for this polymer.[18] Our previous research showed that PVDF has high potential in the thermoset composite welding (TCW). The world-class international patented technology showed great potential for cost saving in the joining and repairing of composite materials and represents the "Next-Generation" assembly technology for aerospace composite structures.[19] However, the poor creep stability has hampered the application in TCW.

In this research, a phase inversion technique was used to fabricate PVDF/multiwall carbon nanotubes (MWCNTs) nanocomposites. The phase inversion technique is a mature method to fabricate membranes.[20–27] Although solvent is still used in this method, the solvent is removed into the antisolvent (water), and could be recycled due to the big difference in the evaporation temperature between the solvent *N*-methyl-2-pyrrolidone (NMP) (about 200°C) and water (about 100°C). Therefore, the phase inversion method used in our current study is certainly an environmentally benign method. During the fabrication, the solidification of the nanocomposites film is very quick, which can avoid MWCNTs reagglomeration, and shorten the fabrication time. A detailed procedure can be seen in the experimental section. The additional advantages of the phase inversion technique include enabling easy preparation of nanocomposites with high content of MWCNTs [1] and improving the dispersion of MWCNTs within the polymer matrix at the same time [2]. The nanocomposites with high content of MWCNTs can then be used as a master-batch material to mass-produce nanocomposite in a more traditional melt-blend process, which is compatible with potential industrial applications. The results will be published in a separate publication.

Because of their highly hydrophobic character, MWCNTs are chemically inert and remain indispersible in almost all solvents (including molten polymers and monomers). Hence, they do not interact strongly with polymer chains[28,29] and surface functionalization of MWCNTs is necessary to achieve high performance. In this present work, a long chain grafted PVDF is used to fine tune the interface between the matrix and MWCNTs.

MATERIALS AND METHODS

Materials

PVDF (Kynar 741, powder) and maleic anhydride grafted PVDF (MAH-graft-PVDF, Kynar ADX-161) named from here on as ADX were kindly supplied by Arkema (Australia, New Zealand). The MWCNTs with diameter of 10–30 nm (mainly around 20 nm) were purchased from Tsinghua University, China. Analytical grade NMP and H_2O_2 were used as solvents and purchased from Aldrich.

Functionalization of MWCNTs with hydroxyl group

A lot of research has shown that MWCNTs with hydroxyl group can be obtained by a hydrogen peroxide treatment.[30–33] To guarantee that the hydroxyl groups will attach onto the MWCNTs surface, the procedure of functionalization used in this current study followed the reference.[33] The pristine MWCNTs were refluxed in HCl (4 : 1) for 4 h at 80°C for purification. The samples were then extracted several times by filtration, until the solution reached a pH value of 7. The treated MWCNTs (t-MWNTs) were then immersed and refluxed in hydrogen peroxide for 65 h at 60°C to attach hydroxyl groups onto the side wall of MWNTs.[33]

Nanocomposites preparation by phase inversion technique

The procedure for fabrication of the nanocomposites was as follows: (1) MWCNTs were dispersed in solvent NMP with strong magnetic stirring and ultrasonic treatment (60 kHz, 1.5 h). At the same time, the polymer, PVDF, was dissolved in NMP to form PVDF solution (the ratio of PVDF and solvent was

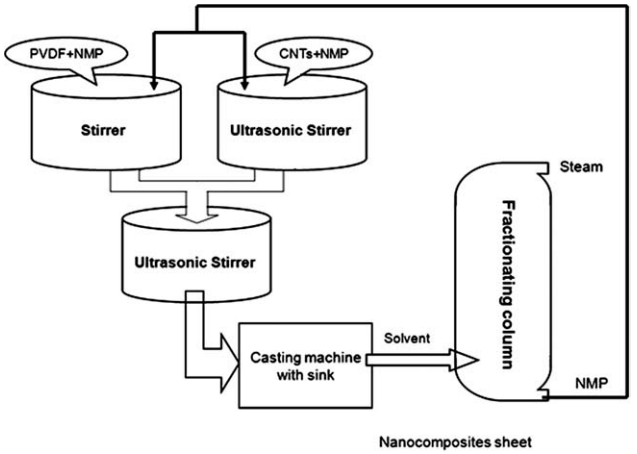

Figure 1 The schematic flow diagram of processing.

1 : 5 by weight); (2) The MWCNTs dispersion and the PVDF solution were mixed together again with strong magnetic stirring and ultrasonic treatment; (3) The mixed solution was poured onto a glass plate, and then compressed with another glass plate to a thickness of about 50 micro; (4) the glass plates were placed into deionized water (the antisolvent to NMP), which caused the film to solidify in several minutes. The wet films were then dried in a vacuum oven for 72 h at 80°C (to avoid the remnant of the solvent). For samples with the addition of ADX, an NMP solution of ADX (the ratio of ADX and solvent was 1 : 10 by weight) was firstly added into MWCNTs liquid with magnetic stirring and ultrasonic treatment for 3 h to let the maleic anhydrate groups react with the hydroxyl groups, and then PVDF-NMP liquid was added. Finally, the dried MWCNTs nanocomposite films were compression moulded at a temperature and pressure of 200°C and 5.0 MPa, respectively. The thickness of the compression-molded films was about 0.5 millimetres.

Although it seems that the above mentioned procedure is very complicate and labor intensive in the laboratory scale, actually it can be mass-produced by the procedure showed schematically in Figure 1. Due to the character of NMP, the solvent can be easily recycled using water. Through the good corporation of the each step, the procedure can form a complete close cycle and work automatically. Except the addition of PVDF and MWCNTs, no more labor is needed. After the addition of the NMP at the start, almost no more NMP is needed, so the fabrication procedure is benign to the environment. The energy from the steam can be used to help drive the stirrer or dissolve polymer, and hence can save energy. In all, the method used in this research is compatible with potential industrial applications and environment-friendly.

As summarized in Table I, various blend formulations were prepared and analyzed.

Characterization

The ultrathin TEM samples (about 50 to 100 nm in thickness) were cut on a Leica EM UC6 ultramicrotome (Leica Microsystems, Wetzlar, Germany), and then investigated by using a Philips Tecnai F20 transmission electron microscope (TEM) equipped with a field emission gun (FEG) at 200 kV. Digital images were acquired by a Gatan CCD camera and then processed by Digital Micrograph v3.9.1 (Gatan, Inc).

DSC tests were conducted by means of a TA Q20 differential scanning calorimeter. In the tests, samples of about 5 mg were heated to 200°C at a rate of 10°C/min under a nitrogen atmosphere and held at 200°C for 5 min to eliminate the thermal history. Afterward, the samples were cooled to 20°C at a rate of 20°C/min, held about 3 min at 20°C, and then heated again to 200°C at a heating rate of 10°C/min. The temperature and heat flow scales were calibrated using the melting of high-purity indium and zinc samples before testing.

ATR-FTIR spectrum was obtained using a Nicolet 5700 ART spectrometer with an average of 200 scans in the range 400–4000 cm^{-1} to obtain the crystal structural for the nanocomposites.

The DMA (tension deformation) was carried out using a TA Instruments Q800 DMA. All the samples were measured over a temperature range of −100°C to 150°C at a heating rate of 3°C/min and at a frequency of 1 Hz. The dimensions of specimens are $30 \times 4 \times 0.5$ mm^3.

The mechanical properties of all materials were measured by an Instron 5584 universal testing machine with a 100 N load cell at a crosshead velocity of 5 mm/min until failure, which equipped with advanced video extensometer. Dumbbells were punched out of the nanocomposites sheets according to ATSM D-638 (type V). At least five samples were measured for each batch. Creep tests were done at the stress level of 20 MPa. The samples were loaded for 2 h according to ASTM D 2990-01. The dimension of specimen is $10 \times 2.5 \times 0.5$ mm^3.

TABLE I
Samples Codification

Sample	Composition
PVDF	PVDF (100% wt)
PN_2	PVDF (100% wt) +MWCNTs (2% wt)
PN_5	PVDF (100% wt) + MWCNTs (5% wt)
PN_5A_2	PVDF (98% wt) + MWCNTs (5% wt) + ADX (2% wt)
PN_5A_5	PVDF (95% wt) + MWCNTs (5% wt) + ADX (5% wt)
PN_5A_{10}	PVDF (90% wt) + MWCNTs (5% wt) + ADX (10% wt)

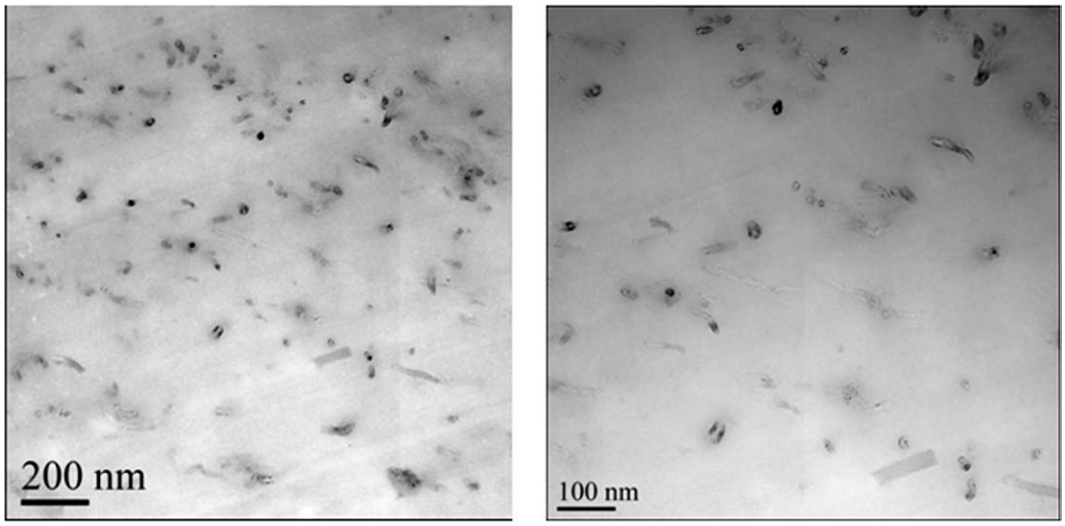

Figure 2 TEM image of PN5 (nanocomposite with 5% wt MWCNTs).

RESULTS AND DISCUSSION

Morphology of the nanocomposites

To assess the dispersion of the carbon nanotubes, the thin sections of the nanocomposites were examined in the TEM. To obtain a true representation of the microstructure, at least 10 positions were investigated for each film, and representative images were taken. Figure 2 shows the typical TEM images of the nanocomposites with 5% wt MWCNTs. It can be seen that the MWCNTs were almost homogeneously dispersed in the PVDF matrix. For traditional melt processing, it is very hard to achieve such good dispersion at this MWCNTs concentration, which is a big step.

Several factors are believed to contribute to the good dispersion of MWCNTs in the PVDF matrix: First, it is known that the solution blending method is an easy way to achieve good dispersion, especially with ultrasonic treatment and magnetic stirring.[17,34] The solvent NMP used in this research has good solubility with MWCNTs, because it has high values for β (the hydrogen bond acceptance basicity), negligible values for α (the hydrogen bond donation parameter of Taft and Kamlet), and high values for π* (solvochromic parameter).[35,36] Second, the chemical treatment which attached hydroxyl functional groups to the surface helped the dispersion of MWCNTs in the solvent and hence formed a stable suspension. Third, the fast phase separation method used in this research avoided the drawback of the traditional solvent casting method, which needs much longer time to evaporate the solvent and may result in reagglomeration during evaporation.

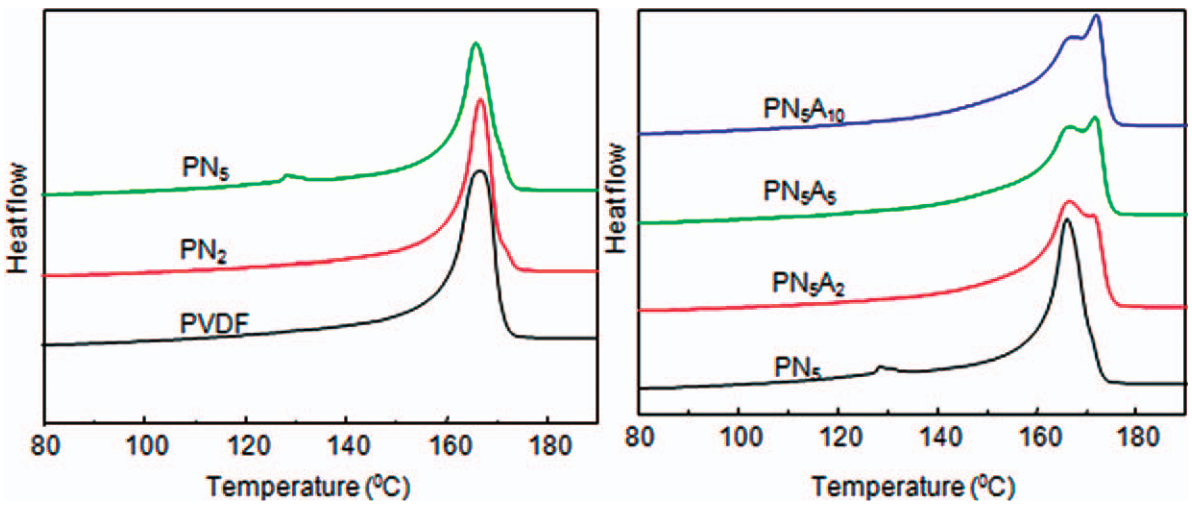

Figure 3 Non-isothermal DSC scans of PVDF and its CNTs nanocomposites (the first heating curve). [Color figure can be viewed in the online issue, which is available at wileyonlinelibrary.com.]

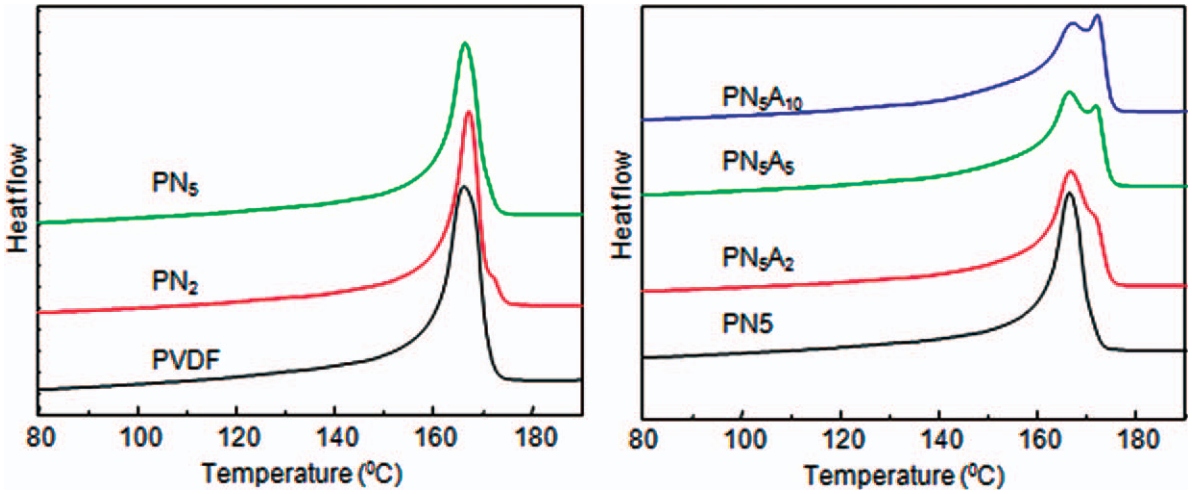

Figure 4 Non-isothermal DSC scans of PVDF and its CNTs nanocomposites (the second heating curves). [Color figure can be viewed in the online issue, which is available at wileyonlinelibrary.com.]

Crystallization behavior and crystal structure

Some research results show that MWCNTs can act as a nucleating agents during the crystallization process of semicrystalline polymers such as polypropylene (PP),[37,38] polyethylene (PE),[39] and poly(ethylene terephthalate) (PET).[40] As a result, the rate of crystallization of the polymer increases, and in most cases the melting temperature also increases.

Figures 3 and 4 show the first and second DSC heating curves for PVDF and its nanocomposites. DSC results of the pure PVDF and nanocomposites are summarized in Table II. PVDF had a melting temperature around 166°C. It seems that the addition of MWCNTs did not significantly alter the melting behavior, only causing a small decrease of the ΔH_m and a small change of the T_m both for the first and second heating curves. The addition of the long chain macromolecules, ADX, had obvious effects on the melting behavior. It can be seen that the ΔH_m decreased a little with the addition of ADX. Another profound change is the increase of melting temperature and the appearance of multimelting behavior, which is related with the appearance of β phase. Huang et al.[41] also reported the same multimelting behavior, and they believe the lower melting peak is attributed to α-phase while the higher one to the β phase as assigned from WXRD data. Double or multiple melting behavior has been investigated extensively and a number of possibilities to explain this phenomenon have been proposed as follows: (1) the presence of more than one crystal form (polymorphism); (2) the presence of different morphologies (lamellar thickness, distribution, perfection, or stability); (3) the presence of melting, recrystallization, and remelting processes during the DSC heating; (4) physical ageing and/or relaxation of the rigid amorphous fraction; (5) different molecular weight species, and so on.[42,43]

To verify the crystal structures of our nanocomposites, ATR-FTIR was conducted, and the result is shown in Figure 5.

The formation of β phase was confirmed by the absorption peaks in FTIR spectra. The α-phase PVDF bands at 974, 795,764, and 614 cm^{-1} can be clearly observed in pure PVDF as well as in all PCNs. β-phase PVDF bands are observed at 840 cm^{-1} in the nanocomposites, indicating a change in the crystalline morphology.[44]

The fraction of β-phase in the nanocomposites was determined from the FTIR scans as:

$$F(\beta) = \frac{A_\beta}{1.3A_\alpha + A_\beta},$$

where A_α and A_β are the absorbances in FTIR spectrum corresponding to the 764 and 840 cm^{-1} bands, respectively.[45] The result is shown in Table III.

A lot of research showed that the addition of the nanofillers will induce the β-phase PVDF.[46–49] It can

TABLE II
DSC Results from First-Heating and Second-Heating Thermograms

	First round		Second round	
Sample	ΔH_m (J/g)	T_m (°C)	ΔH_m (J/g)	T_m (°C)
PVDF	42.97	166.76	43.07	166.14
PN_2	41.04	166.92	40.69	167.14
PN_5	40.53	165.96	40.19	166.42
PN_5A_2	37.73	166.41	37.63	166.62
PN_5A_5	38.90	171.63	38.86	166.38
PN_5A_{10}	38.64	171.85	38.30	172.05

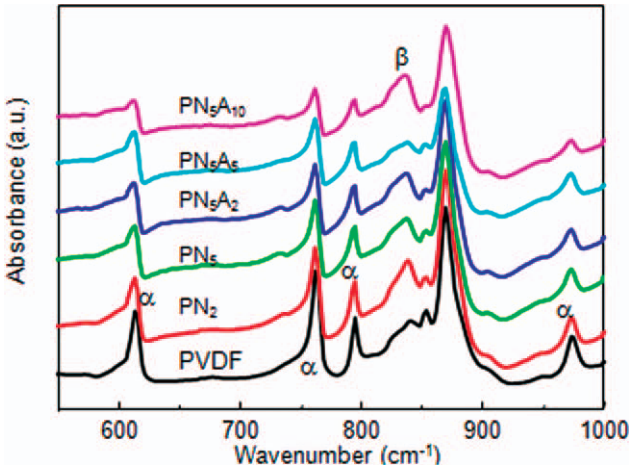

Figure 5 ART-FTIR spectra of PVDF and its CNTs nanocomposites. [Color figure can be viewed in the online issue, which is available at wileyonlinelibrary.com.]

be seen that the addition of MWCNTs indeed induced the β-phase PVDF. The reason is believed to be the fact that MWCNTs surface has zigzag carbon atoms and those atoms match with the all-trans conformation of β-phase PVDF, and as a result induce crystallization of PVDF in the β polymorphic structure.[50] However, other nanofiller with different form, such as layered silicate, can induce β-phase PVDF too. So the nature of the nanofiller inducing β polymorphic structure is not clear yet. On the basis of the value of $F(\beta)$ calculated from the FTIR spectra, the addition of ADX did not increase the amount of β-phase significantly. However, the addition of ADX did create an additional melting peak belonging to the β-phase as detected by DSC. The reason for this phenomenon is that more β-phase was formed due to melt-recrystallization during the DSC heating run. To verify this assumption, DSC tests on sample PN_5A_{10} were conducted using different heating rates (Fig. 6). It can be seen that with the increase in heating rate, the lower melting peak that represents the α-phase became stronger, while the higher melting peak that represents the β-phase became weaker. With the increase of heating rate, less time is available for melt recrystallization and thus less β-phase will be formed, leading to the weaker higher melting peak (β-phase) and a stronger lower melting peak (α-phase). It can also be seen that the addition of ADX facilitated the development of β-phase because the ADX can increase the interaction between the MWCNTs and PVDF polymer. Manna et al.[50] also reported that in functionalized MWCNTs composites, the formation of β-phase is completed at higher F- MWCNTs concentration due to specific interaction, and in the unfunctionalized MWCNTs, the partial β-phase formation is due to the lack of any specific interaction.

TABLE III
Fraction of β-Phase, $F(\beta)$, Calculated from FTIR Spectra

Sample	$F(\beta)$(%)
PVDF	0
PN_2	41.48
PN_5	40.96
PN_5A_2	42.27
PN_5A_5	39.48
PN_5A_{10}	45.53

Dynamic mechanical behavior

In dynamic mechanical (DMA) testing, the sample is subjected to repeated small-amplitude strains in a cyclic manner. The storage modulus (E'), the loss modulus (E'') and the loss tangent (tan $\delta = E''/E'$) are measured. E' is a measure of the energy stored elastically whereas E'' is a measure of the energy lost as heat. Tan δ is also called damping and it indicates how efficiently the material loses energy to molecular rearrangements and internal friction. The tan δ curve reveals the existence of various types of transitions in the polymer sample.[51]

Figure 7 shows the storage moduli of PVDF and its nanocomposites. The storage modulus of PVDF was enhanced by the addition of MWCNTs as well as ADX over the temperature range from −100°C to 150°C. Reinforcement was better at low-temperature regions than high-temperature regions.

Figure 8 shows the tan δ curves of PVDF and its nanocomposites. These curves show a broad peak near −30°C for both PVDF and its nanocomposites, which corresponds to the T_g of PVDF. No significant change in the T_g was observed by the addition of MWCNTs and ADX. This may be explained by the fact that MWCNTs act as nucleation sites and are

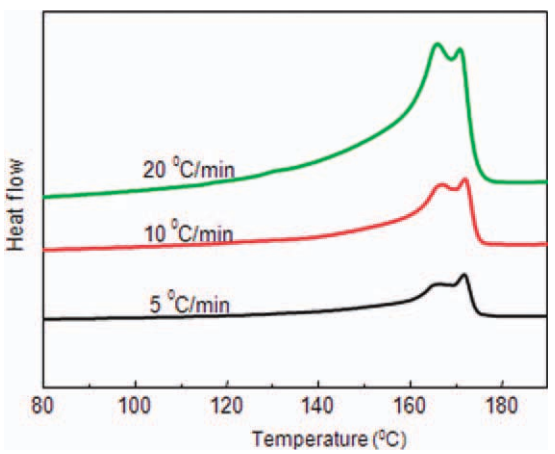

Figure 6 Non-isothermal DSC scans of PN5A10 nanocomposite (different heating rates). [Color figure can be viewed in the online issue, which is available at wileyonlinelibrary.com.]

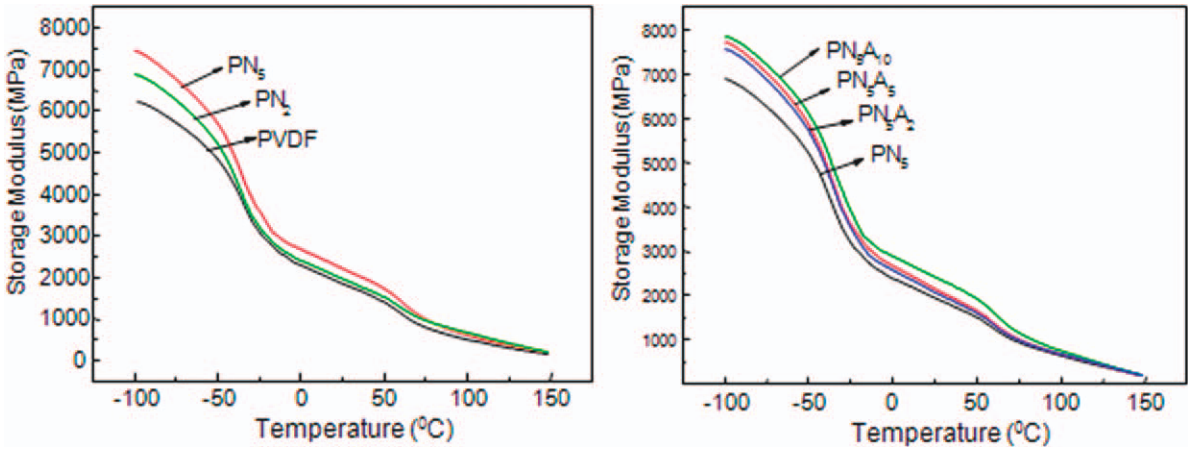

Figure 7 Temperature dependence of the storage modulus for PVDF and its CNTs nanocomposites. [Color figure can be viewed in the online issue, which is available at wileyonlinelibrary.com.]

preferentially associated with the crystalline regions while the ADX prefers to locate in the interface. Consequently, they influence the crystallites and interface rather than the amorphous region which is responsible for T_g. This also provides an explanation for the significant changes with the addition of MWCNTs in the high temperature transition (α) around 90°C, which was ascribed to the liberation of PVDF chains in the crystalline regions.[18]

Mechanical properties

Tensile measurements and creep test were carried out to determine the mechanical properties of the PVDF nanocomposites. Typical stress–strain curves at 5 mm/min for all nanocomposites are shown in Figure 9, and the mechanical properties calculated from the stress–strain curves are shown in Table IV. The results show that Young's modulus and tensile strength increase steadily with the addition of the MWCNTs and ADX. However, the elongation at break decreases obviously. Typical creep strain curves are shown in Figure 10, which shows that the addition of MWCNTs reduces the creep strain. However, the interfacial modifier agent hasn't significantly influence on the creep strain.

The addition of MWCNTs increase the storage modulus, Young's modulus, and tensile strength, and reduces the creep strain, which suggest that the MWCNTs works as reinforcing agent here. With the addition of interfacial modifier ADX, the storage modulus, Young's modulus, and tensile strength increase further. However, the creep strain hasn't obvious decrease, and the reason is due to the difference response of the nanocomposites to the different stimulus, and different structures dominated the properties for the tensile and creep test.

For tensile test, the stress transfer is the key point for the improvement of the Young's modulus due to the fast deformation rate. So the improvement of the interaction affected the Young's modulus significantly. However, for the creep test, the network

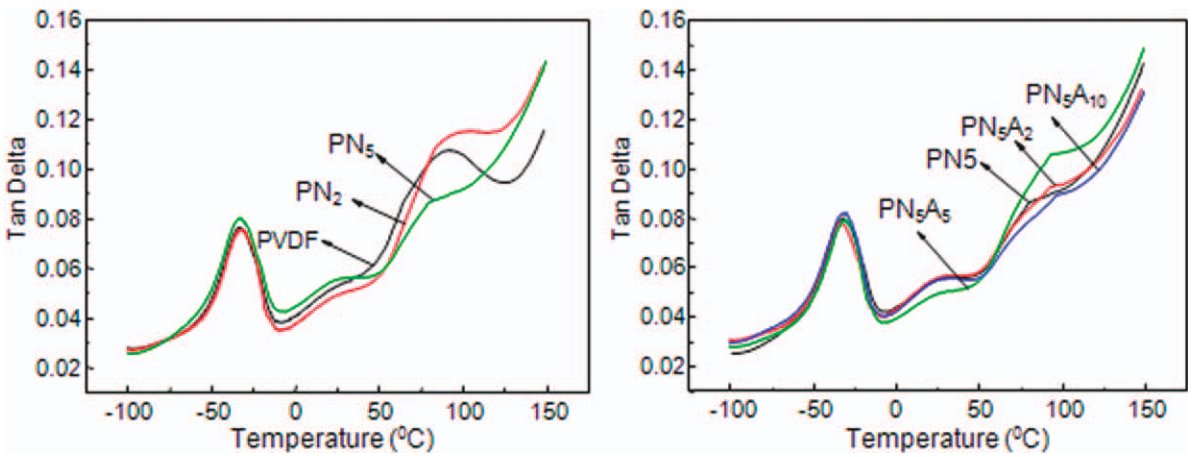

Figure 8 Tan δ as a function of temperature for PVDF and its CNTs nanocomposites. [Color figure can be viewed in the online issue, which is available at wileyonlinelibrary.com.]

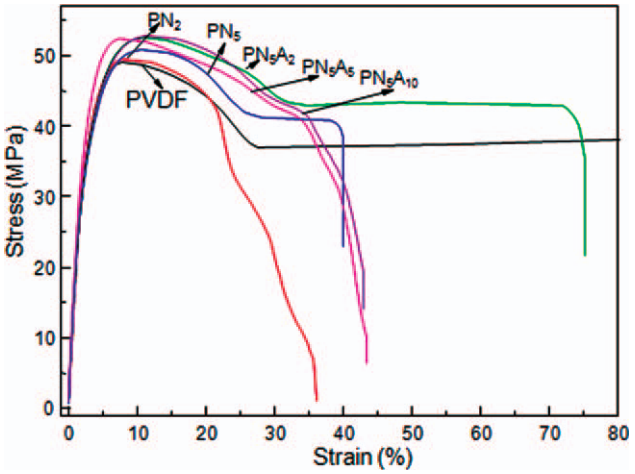

Figure 9 Typical stress–strain curves of PVDF nanocomposites. [Color figure can be viewed in the online issue, which is available at wileyonlinelibrary.com.]

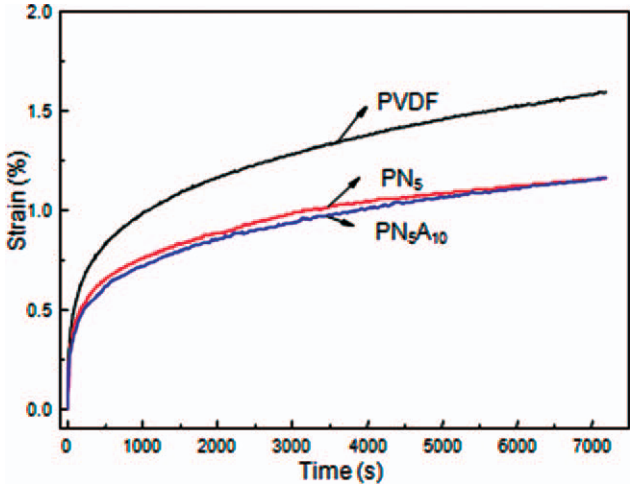

Figure 10 Tensile creep strain vs. test duration-curves of PVDF and its nanocomposites under 20 MPa. [Color figure can be viewed in the online issue, which is available at wileyonlinelibrary.com.]

structure played the key role due to the slow deformation rate. Research has shown that the introduction of nanofiller can improve creep stability.[52–55] For the improvement of creep stability by the addition of nanofillers, the reduction of the chain mobility due to the presence of the nanofillers provide an effective explanation for the enhancement of the material stability under creep condition.[53] However, from the DMA test, no significant change in the T_g was observed by the addition of MWCNTs and ADX, which meant that there was not significant changes about the chain mobility. So the reduction of the chain mobility cannot explain the improvement of the creep stability. It was thought the improvement was due to the network structures formed by the MWCNTs. Because of the high aspect ratio and good mechanical properties, the normal state of MWCNTs is bent, and with the increase of the amount, some MWCNTs connect by physical contact and form network structure, which can be imagined as claw with a lot of bent fingers, which dominated the creep behavior. So the 5% MWCNTs decreased the creep strain significant. However, further improvement of the interaction between the PVDF matrix and the MWCNTs did not show significant improvement for the creep stability.

TABLE IV
Mechanical Properties from Tensile Testing for PVDF Nanocomposites

Sample	Young's modulus (GPa)	Tensile strength (MPa)	Elongation at break (%)
PVDF	1.97 (0.04)	49.3 (0.5)	254.3 (121.2)
PN_2	2.27 (0.13)	50.8 (0.5)	40.8 (10)
PN_5	2.29 (0.16)	50.6 (0.9)	38.3 (10)
PN_5A_2	2.37 (0.05)	51.7 (1.5)	46.1 (17)
PN_5A_5	2.61 (0.09)	52.8 (0.5)	30.8 (10)
PN_5A_{10}	2.79 (0.05)	52.8 (0.4)	33.7 (9)

CONCLUSION

Quasi-homogenous PVDF/MWCNTs nanocomposites have been fabricated using the phase inversion technique. DSC and ATR-FTIR results showed that the addition of MWCNTS induced β-phase PVDF, and further addition of MWCNTs did not change the melting behavior and crystal structures. The addition of long chain macromolecules, ADX, did not alter the crystal structure according to the ATR-FTIR test, however, the melting behavior changed significantly. Multiple melting behavior occurred, which may have been caused by the melt recrystallization during the DSC test. DMA results showed that the addition of MWCNTs and ADX increased the storage modulus, and the reinforcement effect was more profound at low temperature regions than high temperature regions. No obvious change in the T_g was observed by the addition of MWCNTs and ADX. Tensile tests showed that the Young's modulus and tensile strength increase with the addition of the MWCNTs and ADX. Creep test showed that the addition of MWCNTs can increase the creep stability. However, the interfacial modification here didn't increase the creep stability significantly.

The authors thank the Arkema for the supply of PVDF and MAH-graft-PVDF free of charge. They are also heavily indebted to Mr. Graham Ruhle from the Mechanical and Mining Engineering N.A.T.A. endorsed Mechanical Testing laboratory of the University of Queensland for help with the tensile testing, and the editing work from Mr. S. Davey.

References

1. Iijima, S. Nature 354, 56, 1991.
2. Wong, E. W.; Sheehan, P. E.; Lieber, C. M. Science 1997, 277, 1971.
3. Yu, M. F.; Lourie, O.; Dyer, M. J.; Moloni, K.; Kelly, T. F.; Ruoff, R. S. Science 2000, 287, 637.
4. Xie, S. S.; Li, W. Z.; Pan, Z. W.; Chang, B. H.; Sun, L. F. J Phys Chem Solids 2000, 61, 1153.
5. Hata, K.; Futaba, D. N.; Mizuno, K.; Namai, T.; Yumura, M.; Iijima, S. Science 2004, 306, 1362.
6. Zhang, H.; Zhang, Z. Eur Polym J 2007, 43, 3197.
7. Song, L.; Zhang, H.; Zhang, Z.; Xie, S. S. Compos A 2007, 38, 388.
8. Xie, X. L.; Aloys, K.; Zhou, X. P.; Zeng, F. D. J Therm Anal Calorim 2003, 74, 317.
9. Xie, X.-L.; Mai, Y.-W.; Zhou, X.-P. Mater Sci Eng R 2005, 49, 89.
10. Zhang, B.; Dong, X. M.; Fu, R. M.; Zhao, B.; Zhang, M. Q. Compos Sci Technol 2008, 68, 1357.
11. Wu, X. B.; Zhang, M. Q.; Wang, J.; Tian, Q. J Korean Phys Soc 2010, 56, 1103.
12. Coleman, J. N.; Khan, U.; Gun'ko, Y. K. Adv Mater 2006, 18, 689.
13. Ma, W. J.; Liu, L. Q.; Zhang, Z.; Yang, R.; Liu, G.; Zhang, T. H.; An, X. F.; Yi, X. S.; Ren, Y.; Niu, Z. Q.; Li, J. Z.; Dong, H. B.; Zhou, W. Y.; Ajayan, P. M.; Xie, S. S. Nano Lett 2009, 9, 2855.
14. McClory, C.; Chin, S. J.; McNally, T. Aust J Chem, 2009, 62, 762.
15. Park, S. J.; Cho, M. S.; Lim, S. T.; Choi, H. J.; Jhon, M. S. Macromol Rapid Commun 2003, 24, 1070.
16. Chen, G. X.; Li, Y. J.; Shimizu, H. Carbon 2007, 45, 2334.
17. Moniruzzaman, M.; Winey, K. I. Macromolecules 2006, 39, 5194.
18. Priya, L.; Jog, J. P. J Polym Sci Part B: Polym Phys 2002, 40, 1682.
19. Hou, M.; Beehag, A.; Yuan, Q. Welding techniques for polymer or polymer composite components. Advanced Composite Structures June 2004: KR 1020047001306.
20. Kim, K. M.; Park, N. G.; Ryu, K. S.; Chang, S. H. Electrochim Acta 2006, 51, 5636.
21. Hwang, Y. J.; Nahm, K. S.; Kumar, T. P.; Stephan, A. M. J Membr Sci 2008, 310, 349.
22. Hwang, J.; Jeong, S. K.; Nahm, K. S.; Stephan, A. M. Eur Polym J 2007, 43, 65.
23. Jin, C.; Liu, J.; Li, L. H.; Bai, Y. H. J Membr Sci 2009, 341, 233.
24. Blanco, J. F.; Sublet, J.; Nguyen, Q. T.; Schaetzel, P. J Membr Sci 2006, 283, 27.
25. Buonomenna, M. G.; Macchi, P.; Davoli, M.; Drioli, E. Eur Polym J 2007, 43, 1557.
26. Mago, G.; Kalyon, D. M.; Fisher, F. T. J Nanomater 2008, 2008.
27. Mago, G.; Fisher, F. T.; Kalyon, D. M. J Nanosci Nanotechnol 2009, 9, 3330.
28. Vigolo, B.; Mamane, V.; Valsaque, F.; Le, T. N. H.; Thabit, J.; Ghanbaja, J.; Aranda, L.; Fort, Y.; McRae, E. Carbon 2009, 47, 411.
29. Yang, Y. K.; Xie, X. L.; Wu, J. G.; Yang, Z. F.; Wang, X. T.; Mai, Y. W. Macromol Rapid Commun 2006, 27, 1695.
30. Peng, Y.; Liu, H. W. Ind Eng Chem Res 2006, 45, 6483.
31. Datsyuk, V.; Kalyva, M.; Papagelis, K.; Parthenios, J.; Tasis, D.; Siokou, A.; Kallitsis, I.; Galiotis, C. Carbon 2008, 46, 833.
32. Wang, L.; Xing, D. M.; Zhang, H. M.; Yu, H. M.; Liu, Y. H.; Yi, B. L. J Power Sources 2008, 176, 270.
33. Han, J. T.; Kim, S. Y.; Woo, J. S.; Lee, G. W. Adv Mater 2008, 20, 3724.
34. Kim, H. M.; Kim, K.; Lee, S. J.; Joo, J.; Yoon, H. S.; Cho, S. J.; Lyu, S. C.; Lee, C. J. Curr Appl Phys 2004, 4, 577.
35. Ausman, K. D.; Piner, R.; Lourie, O.; Ruoff, R. S.; Korobov, M. J Phys Chem B 2000, 104, 8911.
36. Marcus, Y. J Solution Chem 1991, 20, 929.
37. Valentini, L.; Biagiotti, J.; Lopez-Manchado, M. A.; Santucci, S.; Kenny, J. M. Polym Eng Sci 2004, 44, 303.
38. Leelapornpisit, W.; Ton-That, M. T.; Perrin-Sarazin, F.; Cole, K. C.; Denault, J.; Simard, B. J Polym Sci Part B: Polym Phys 2005, 43, 2445.
39. Haggenmueller, R.; Fischer, J. E.; Winey, K. I. Macromolecules 2006, 39, 2964.
40. Anand, K. A.; Agarwal, U. S.; Joseph, R. Polymer 2006, 47, 3976.
41. Huang, X. Y.; Jiang, P. K.; Kim, C.; Liu, F.; Yin, Y. Eur Polym J 2009, 45, 377.
42. Shan, G.-F.; Yang, W.; Tang, X.-G.; Yang, M.-B.; Xie, B.-H.; Fu, Q.; Mai, Y.-W. Polym Test 2010, 29, 273.
43. Yasuniwa, M.; Tsubakihara, S.; Fujioka, T.; Dan, Y. Polymer 2005, 46, 8306.
44. Patro, T. U.; Mhalgi, M. V.; Khakhar, D. V.; Misra, A. Polymer 2008, 49, 3486.
45. Gregorio, R.; Cestari, M. J Polym Sci Part B: Polym Phys 1994, 32, 859.
46. Buckley, J.; Cebe, P.; Cherdack, D.; Crawford, J.; Ince, B. S.; Jenkins, M.; Pan, J. J.; Reveley, M.; Washington, N.; Wolchover, N. Polymer 2006, 47, 2411.
47. Priya, L.; Jog, J. P. J Appl Polym Sci 2003, 89, 2036.
48. Nam, P. H.; Maiti, P.; Okamoto, M.; Kotaka, T.; Hasegawa, N.; Usuki, A. Polymer 2001, 42, 9633.
49. Levi, N.; Czerw, R.; Xing, S. Y.; Iyer, P.; Carroll, D. L. Nano Lett 2004, 4, 1267.
50. Manna, S.; Nandi, A. K. J Phys Chem C 2007, 111, 14670.
51. Wang, M.; Shi, J.-H.; Pramoda, K. P.; Goh, S. H. Nanotechnology 18, 2007.
52. Siengchin, S.; Karger-Kocsis, J.; Thomann, R. Express Polym Lett 2008, 2, 746.
53. Dorigato, A.; Pegoretti, A. Polym Int 59, 719, 2010.
54. Dorigato, A.; Pegoretti, A.; Kolarik, J. Polym Compos 31, 1947, 2010.
55. Bondioli, F.; Dorigato, A.; Fabbri, P.; Messori, M.; Pegoretti, A. Polym Eng Sci 2008, 48, 448.